



HAL
open science

Study of middle infrared difference frequency generation using a femtosecond laser source in LGT

Elodie Boursier, Giedre Marja Archipovaite, Jean-Christophe Delagnes, Stephane Petit, Guilmot Ernotte, Philippe Lassonde, Patricia Segonds, Benoit Boulanger, Yannick Petit, François Légaré, et al.

► **To cite this version:**

Elodie Boursier, Giedre Marja Archipovaite, Jean-Christophe Delagnes, Stephane Petit, Guilmot Ernotte, et al.. Study of middle infrared difference frequency generation using a femtosecond laser source in LGT. *Optics Letters*, 2017, 42 (18), pp.3698-3701. 10.1364/OL.42.003698 . hal-01597693

HAL Id: hal-01597693

<https://hal.science/hal-01597693>

Submitted on 24 Nov 2023

HAL is a multi-disciplinary open access archive for the deposit and dissemination of scientific research documents, whether they are published or not. The documents may come from teaching and research institutions in France or abroad, or from public or private research centers.

L'archive ouverte pluridisciplinaire **HAL**, est destinée au dépôt et à la diffusion de documents scientifiques de niveau recherche, publiés ou non, émanant des établissements d'enseignement et de recherche français ou étrangers, des laboratoires publics ou privés.

Title:

Study of middle infrared difference frequency generation using a femtosecond laser source in LGT

Authors:

Elodie Boursier, Giedre Marija Archipovaite, Jean-Christophe Delagnes, Stéphane Petit, Guilmot Ernotte, Philippe Lassonde, Patricia Segonds, Benoît Boulanger, Yannick Petit, François Légaré, Dmitry Roshchupkin, and Eric Cormier

Manuscript

The original publication may be found at:

Journal: Optics Letters, Vol. 42, No. 18 / 2017 / 3698-3701

DOI: <https://doi.org/10.1364/OL.42.003698>

Study of Middle Infrared Difference Frequency Generation Using a Femtosecond Laser Source in LGT

ELODIE BOURSIER^{1,2,3,*}, GIEDRE MARIJA ARCHIPOVAITE³, JEAN-CHRISTOPHE DELAGNES³, STEPHANE PETIT³, GUILMOT ERNOTTE⁴, PHILIPPE LASSONDE⁴, PATRICIA SEGONDS^{1,2}, BENOIT BOULANGER^{1,2}, YANNICK PETIT^{3,5}, FRANÇOIS LEGARE⁴, DMITRY ROSHCHUPKIN⁶ AND ERIC CORMIER³

¹ Université Grenoble Alpes, Institut Néel, F38402 Grenoble Cedex 9, France

² CNRS, Institut Néel, F38402 Grenoble Cedex 9, France

³ CELIA, Université de Bordeaux – CNRS – CEA, 33405 Talence, France

⁴ INRS, INF, ALLS, Varennes, Québec, Canada

⁵ ICMCB, Université de Bordeaux, CNRS, 33600 Pessac, France

⁶ Institute of Microelectronics Technology, Russian Academy of Sciences, Chernogolovka, 142432, Russia

*Corresponding author: elodie.boursier@u-bordeaux.fr

Received XX Month XXXX; revised XX Month, XXXX; accepted XX Month XXXX; posted XX Month XXXX (Doc. ID XXXXX); published XX Month XXXX

We demonstrate phase-matched difference frequency generation in the emerging nonlinear crystal $\text{La}_3\text{Ga}_{5.5}\text{Ta}_{0.5}\text{O}_{14}$ (LGT). Continuously tunable wavelengths between 1.4 and 4.7 μm are generated by using femtosecond sources. We also report on measurements of optical damage threshold in the femtosecond regime and on the nonlinear refractive index n_2 .

© 2017 Optical Society of America

OCIS codes: (190.4400) Nonlinear optics, materials; (190.4410) Nonlinear optics, parametric processes; (320.7090) Ultrafast lasers.

<http://dx.doi.org/XX.XXXX/XX.XX.XXXXXX>

Many applications such as linear and multidimensional infrared spectroscopy require the generation of widely tunable femtosecond pulses with high average power covering the atmospheric transmission window (3 – 5 μm). Furthermore, long wavelength few-cycle pulses are of prime importance in strong field physics especially when carrier-envelope phase effects are investigated. Since too few laser materials with sufficient bandwidth in this spectral domain has been developed yet, the only alternative is phase-matched difference frequency generation (DFG) and optical parametric amplification (OPA) in nonlinear crystals pumped by powerful high beam quality laser sources. Both DFG and OPA covering the SWIR (1.4 - 3 μm) and part of the MIR (3 – 5 μm) bands have been successfully demonstrated in widespread nonlinear crystals such as $\beta\text{-BaB}_2\text{O}_4$ (BBO), KTiOAsO_4 (KTA), and LiNbO_3 (LNB) [1-11] associated with commercial femtosecond pump laser sources based on Yb^{3+} - or Nd^{3+} -doped

materials ($\sim 1 \mu\text{m}$) or Ti:Sa laser ($\sim 0.8 \mu\text{m}$). Recently, we identified Langatate $\text{La}_3\text{Ga}_{5.5}\text{Ta}_{0.5}\text{O}_{14}$ (LGT), initially known for its piezoelectric properties, as another promising nonlinear crystal with a transparency window ranging from 0.3 up to 6 μm [12, 13]. Czochralski growth method may provide centimeter-size Langatate crystals with very good optical quality and homogeneity. LGT belongs to the trigonal 32 point group and is a positive uniaxial crystal. The Sellmeier coefficients retrieved by the sphere method are reported in [13] with a nonlinear coefficient $d_{11} = 2.4 \pm 0.4 \text{ pm/V}$ at $\lambda = 0.67 \mu\text{m}$. Optical damage appeared at 4.3 GW/cm^2 , i.e. 21.7 J/cm^2 , when illuminated by a $1.064 \mu\text{m}$ (10 Hz, 5 ns) Nd:YAG laser with a $220 \mu\text{m}$ beam diameter [13]. Calculations showed that a LGT slab cut along a phase-matching (PM) direction ($\theta_{PM} = 56^\circ$ and $\varphi_{PM} = 90^\circ$) and pumped at $0.967 \mu\text{m}$ can generate broadband pulses spanning from 1.5 to 3.5 μm [13].

In this Letter, we report to the best of our knowledge, on the first study of middle infrared difference frequency generation in LGT crystal using ~~ultrashort femtosecond pulses in the femtosecond regime~~. The investigations carried out at low intensity in this Letter highlight the potentiality of LGT as a novel nonlinear crystal for DFG and optical parametric amplification in the middle infrared. Two kinds of sources provided the incoming pump and signal beams. One was an amplified continuum generator pumped around $\sim 1 \mu\text{m}$ by using a high-repetition-rate and high-average-power laser based on Yb^{3+} -doped material. The second source was a TOPAS® OPA pumped by a Ti:Sa laser. The tunability of the generated wavelength was measured in the same rotating LGT slab, from three experimental configurations. We also determined the optical damage threshold and the nonlinear refractive index n_2 of LGT.

Our calculations, using Sellmeier coefficients from ref. [13], predict that phase-matched Type-I DFG/OPA ($\lambda_p^o, \lambda_s^e, \lambda_i^e$) can be generated in a LGT slab cut at $\theta_{PM} = 58.3^\circ$ in the y - z plane ($\varphi_{PM} = 90^\circ$) by combining two incoming beams collinearly. It generates a beam continuously tunable while rotating the slab. Here λ_p and λ_s are the incoming pump and signal wavelengths, respectively, while λ_i is the corresponding idler wavelength, with the convention $\lambda_p < \lambda_s \leq \lambda_i$. Then during the DFG/OPA process, the beam at λ_s exhibits an amplification (OPA) while the beam at λ_i is generated (DFG). The superscripts o and e stand for the ordinary and extraordinary waves, respectively.

In order to validate our calculations and to evaluate the full potential of LGT, three different experimental configurations (a), (b) and (c) were implemented, as shown in Fig. 1. In (a), a broadband pump at $\lambda_p = 0.7 \mu\text{m}$ is mixed with a narrowband signal at $\lambda_s = 1.03 \mu\text{m}$. In (b), a narrowband pump at $\lambda_p = 1.03 \mu\text{m}$ is mixed with a broadband signal at $\lambda_s = 1.5 \mu\text{m}$. Finally in (c), a broadband (80 nm) pump at $\lambda_p = 1.3 \mu\text{m}$ and a broadband (135 nm) signal at $\lambda_s = 1.9 \mu\text{m}$ are mixed together.

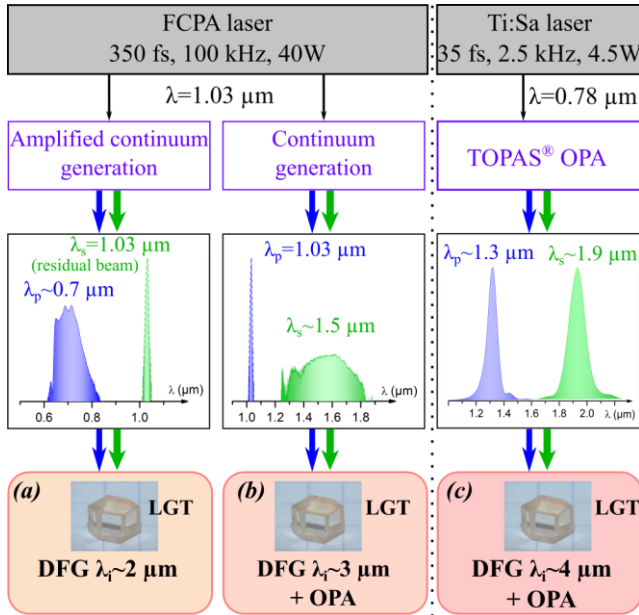


Fig. 1. Schematic drawing of the three experimental configurations (a), (b) and (c), using the same LGT crystal cut at ($\theta_{PM} = 58.3^\circ, \varphi_{PM} = 90^\circ$).

In (a) and (b), we used a homemade Yb^{3+} -doped fiber chirped-pulse amplification (FCPA) source based on a rod-type large mode area fibers operating at 100 kHz. The 350 fs (FWHM) laser pulses emitted at $\lambda = 1.03 \mu\text{m}$ are here considered as narrowband ($\sim 6 \text{ nm}$), and the measured energy was about 60 μJ at the input of the LGT sample. One part of the 1.03 μm beam is smoothly focused in an undoped YAG ($\text{Y}_3\text{Al}_5\text{O}_{12}$) rod in order to generate a broadband continuum (0.6 - 1.8 μm). Out of this continuum, we can either select a broadband (90 nm FWHM) visible beam centered at 0.7 μm using (a), or a broadband (436 nm FWHM) IR spectrum centered at 1.5 μm using (b). Consequently, the weak visible beam was first amplified by OPA in a β -BBO crystal pumped at 0.515 μm (SHG of 1.03 μm) in order to reach about 60 nJ. The 1.5 μm beam energy was less than 5 nJ, and the beam sizes at $1/e^2$ were about 180 μm for both beams in case of (a) and (b). For (c), we used a commercial 2.5 kHz repetition rate and 35 fs pulse width TOPAS[®]

OPA pumped by $\lambda = 0.78 \mu\text{m}$ of a Ti:Sa laser. The incoming beams size at $1/e^2$ was 180 μm with 1 μJ energy level.

Depending on the central wavelength, the spectra of the incoming pump and signal beams are recorded with an Ocean Optics HR2000 spectrometer (0.4 - 1.1 μm , $\Delta\lambda = 1 \text{ nm}$) and a NIRQuest (0.9 - 2.5 μm , $\Delta\lambda = 7 \text{ nm}$). The idler spectra are measured with a Mozza[®] Fastlite[™] monochromator (1 - 5 μm , $\Delta\sigma = 5 \text{ cm}^{-1}$) in (a) and (b), and a homemade scanning monochromator (1.5 - 5 μm , $\Delta\lambda = 2 \text{ nm}$) in (c). Figures 2a, 3a and 4a show spectra of the incoming beams and of the phase-matched idler beam by rotating LGT. Note that for sake of clarity, the measured amplified signal spectra in configuration (b) are not shown.

The LGT slab is cut at the predicted optimal angle $\theta_{PM} = 58.3^\circ$ in the y - z plane, and controlled using X-Rays in backscattering geometry. In order to limit the group-velocity mismatch between the pump and signal beams, a slab thickness of $L = 3.84 \text{ mm}$ was used in the three experiments. It was polished to optical quality and mounted on a rotating stage. The incident angle was measured by using the incident-to-reflected beam angle method. This technique results in $\pm 1^\circ$ error on the measured angle.

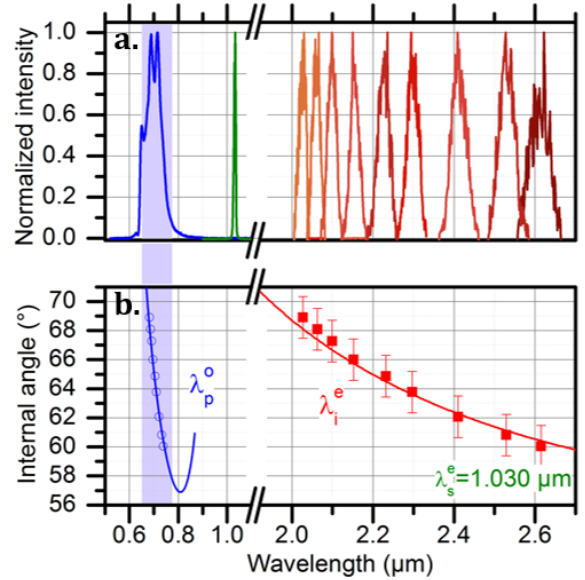


Fig. 2. Experimental data for the generated beam at λ_i (red) using a broadband pump at $\lambda_p = 0.7 \mu\text{m}$ (blue) and a narrowband signal at $\lambda_s = 1.03 \mu\text{m}$ (green) as incoming beams in a LGT slab using configuration (a). a) Incoming and idler beams normalized intensities, and b) internal angles are plotted as a function of the wavelength. Blue circles are the associated selected pump wavelengths, and lines are calculations from ref. [13].

The phase-matching conditions are recovered by determining the wavelength of the maximum value of all recorded spectra. Then we plotted the tuning curves in LGT based on the internal angle as a function of the phase-matching wavelength λ_i (see Figs. 2b, 3b and 4b) and λ_s (see Fig. 3b). Due to the weak signal gain in configurations (a) and (c), it was not possible to observe any significant spectral modification with the spectrometers. However in (c), the corresponding tuning curve was calculated using energy conservation between the measured idler wavelength and the pump set at $\lambda_p = 1.32 \mu\text{m}$, which corresponds to the peak value of the pump spectrum (see dots in Fig. 4b). Based on the same

principle, we also determined in configuration (a) the pump wavelengths from the broadband spectrum shown in Fig. 2a that were combined with the narrowband signal, in order to generate the phase-matched idler wavelengths shown in Fig. 2b.

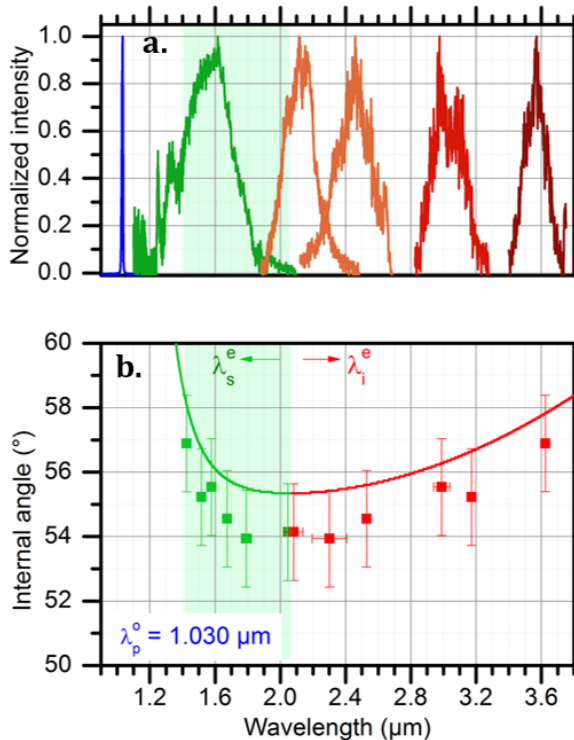


Fig. 3. Experimental data of the idler (red) and signal (green), using a narrowband pump $\lambda_p = 1.03 \mu\text{m}$ (blue) and a broadband signal $\lambda_s = 1.5 \mu\text{m}$ (green) as incoming beams. a) Incoming and idler generated normalized intensities, and b) internal angles are plotted as a function of the wavelength in LGT slab. Lines are calculations after ref. [13].

Figs. 2b, 3b and 4b show that the same LGT slab cut at $\theta_{PM} = 58.3^\circ$ is able to generate or amplify wavelengths between 1.4 and 4.7 μm by tilting the crystal in the y - z plane over 21° with different pump sources. Depending on the pump source, a continuous tunability is demonstrated from 2.1 to 2.6 μm , 1.4 to 3.6 μm , and 3.4 to 4.7 μm . Calculations based on ref. [13] agree very well with our experimental data within the precision of our measurements in the three experimental configurations. For the sake of clarity, in the case of broadband pump and signal (configuration (c)), we have calculated the phase-matching curves (see Fig. 4b) corresponding to three pump wavelengths: $\lambda_{p2} = 1.32 \mu\text{m}$ (maximum of the pump spectrum), $\lambda_{p1} = 1.18 \mu\text{m}$, and $\lambda_{p3} = 1.41 \mu\text{m}$ (wavelengths corresponding to 50 % of pump maximum spectral intensity). All recorded data fit within the internal phase-matching curves.

Note that the measured spectral bandwidth of the idler waves matches with the simulated curve after considering all the incoming experimental parameters, *i.e.* pulse duration, beam sizes, pulse energy, and sample characteristics. Thinner crystal would certainly provide broader spectra at all wavelengths.

In Fig. 5 we compare the spectral range of the generated wavelengths in LGT with that obtained in β -BaB₂O₄ (BBO), KTiOAsO₄ (KTA) and Periodically-Poled LiNbO₃ (PPLN) from refs. [1-11]. The transparency range of each crystal is shown with the dashed white bars and the measured spectral range of the

generated wavelengths through the blue and red colored bars. The later corresponds to cases for which the nonlinear crystals are pumped by two femtosecond commercial laser sources around either 0.8 μm (blue bars) or 1 μm (red bars). Figure 5 points out that the measured spectral ranges of LGT are comparable to that of PPLN when pumped around 1 μm . In comparison BBO and KTA are much more limited in this aspect.

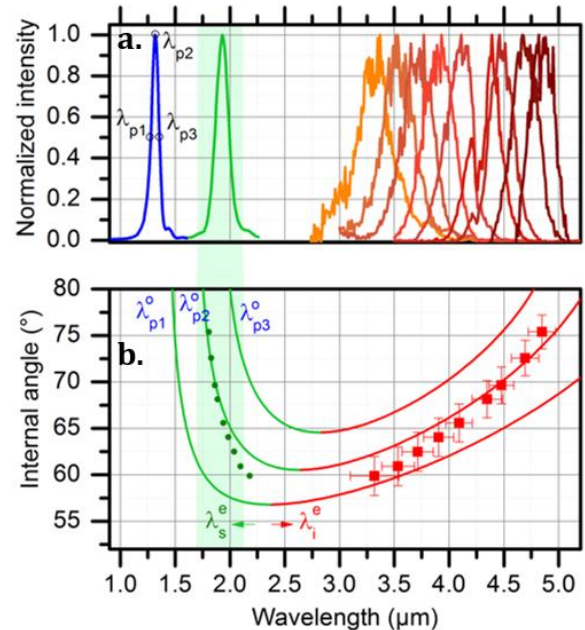


Fig. 4. Experimental data of the idler (red) using a broadband pump $\lambda_p = 1.3 \mu\text{m}$ (blue) and a broadband signal $\lambda_s = 1.9 \mu\text{m}$ (green) as incoming beams. a) Incoming and idler normalized intensities and b) internal angles plotted as a function of the wavelength in LGT slab. Lines are calculations after ref. [13] for three selected quasi-monochromatic pump wavelengths $\lambda_{p1} = 1.18 \mu\text{m}$, $\lambda_{p2} = 1.32 \mu\text{m}$ and $\lambda_{p3} = 1.41 \mu\text{m}$ from the pump spectral width.

The optical damage threshold was studied by using a 500 μm thick slab cut at $\theta = 9^\circ$ in the y - z plane where we found no phase-matching condition [13]. We used a sub-15 fs pulse duration, 100 Hz repetition rate Ti:Sa laser (800 nm) and the same experimental setup as in ref [14].

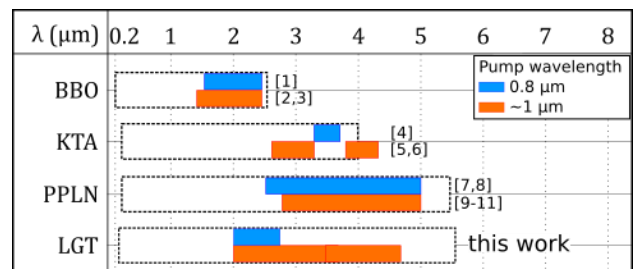


Fig. 5. Transparency ranges (dashed white bars) and measured spectral ranges generated in BBO, KTA, PPLN and LGT when pumped around 0.8 μm (blue bars) and around 1 μm (red bars).

The energy was very low, *i.e.* around 1 μJ , and the beam was tightly focused at the surface of the sample using an off-axis parabola mirror. Accurate calibration and measurement give a $10 \mu\text{m} \pm 5 \%$ beam waist diameter [14]. The LGT slab sits on a 3-axis motorized

translation stage in order to control the optimal focusing position. We adopted a so-called 1-on-1 protocol, *i.e.* one shot per site and ten tested sites per considered fluence, while maintaining a normal incidence and sufficient spacing to avoid crosstalk. The energy, and thus the fluence, were the only varying parameters. A preliminary calibration was achieved with fused silica as a reference material. Then, the LGT crystal was processed to determine the damage probability by increasing the fluence continuously. A fluence of 425 mJ/cm² still led to 0 % damage while the probability reached 80 % at 500 mJ/cm², setting then the optical damage threshold. This result corroborates the optical damage threshold measured in nanosecond regime [13] if corrected for the pulse duration difference [15]. Fig. 6 plots the damage fluence as a function of the nonlinear parameter for widespread nonlinear crystals in the nanosecond regime. LGT is represented by the plain (ns) and light (fs) red disks. The different chemical families of nonlinear crystals are distinguished by different colors.

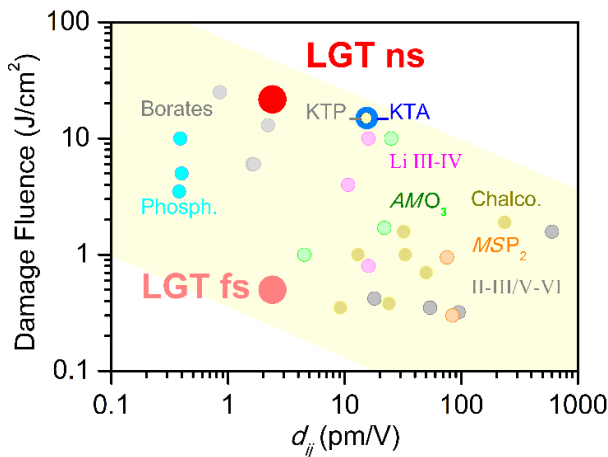


Fig. 6. Damage threshold as a function of the highest nonlinear coefficient d_{ij} for Alkali Metal Oxides (AMO₃), Metal Semiconductor Diphosphide (MSP₂), II-III/V-VI = II/VI and III/V semiconductors, Li III-IV = LiGaS₂, LiInS₂ and LiInSe₂ crystals in the nanosecond regime.

Finally, we directly measured the third-order nonlinear electric susceptibility $\chi_{xxxx}^{(3)}$ of LGT at 0.343 μm from third-harmonic generation performed at the surface of a 820 μm thick slab cut at ($\theta = 57^\circ$, $\varphi = 90^\circ$). For this purpose, we used an Amplitude Systemes t-Pulse[®] oscillator (390 fs, $\lambda_\omega = 1.030 \mu\text{m}$, 9 MHz) with a linear polarization oriented parallel to x-axis of LGT, and implemented the setup described in ref [16]. We took into account the Fresnel losses, the third-harmonic transmission, the nonlinear interaction length and the refractive indices corrections at λ_ω and $\lambda_{3\omega} = \lambda_\omega/3 = 0.343 \mu\text{m}$ [16]. We studied a fused silica slab in the same conditions, to use $\chi_{xxxx}^{SiO_2}(0.343 \mu\text{m}) = 2.48 \times 10^{-22} \text{ m}^2 \cdot \text{V}^{-2}$ from [17] as a reference. We found for LGT that $\chi_{xxxx}(0.343 \mu\text{m}) = 18 \chi_{xxxx}^{SiO_2}(0.343 \mu\text{m}) = (4.5 \pm 0.5) \times 10^{-21} \text{ m}^2 \cdot \text{V}^{-2}$. The nonlinear refractive index n_2 is linked to $\chi_{xxxx}^{(3)}$ by the relation $n_2(\lambda_{3\omega}) = \frac{3\chi_{xxxx}^{(3)}(\lambda_{3\omega})}{4n_0(\lambda_{3\omega})\epsilon_0 c}$ where n_0 stands for the ordinary refractive index of LGT, c is the light speed and ϵ_0 the vacuum dielectric constant. Then we found for LGT that $n_2(0.343 \mu\text{m}) = (6.3 \pm 0.7) \times 10^{-19} \text{ m}^2 \cdot \text{W}^{-1}$, which is about ten times that of BBO and three times that of KTA or PPLN at 0.780 μm [13,18]. It means that LGT may be associated with stronger self-focusing due to Kerr effect and then

lead to potential damage. However, it is worth to mention that LGT can be grown in the largest sizes and the greatest homogeneity [13] if compared to KTA for which inhomogeneity is a real issue.

In conclusion, we performed the optical characterization of LGT in the femtosecond regime. Three experimental configurations of DFG/OPA were studied and led to the angular tuned generation of wavelengths ranging between 1.2 and 4.7 μm . These results show that LGT stands as a serious competitor of BBO, KTA and PPLN for parametric generation in the atmospheric transmission window. In particular the high optical damage thresholds of LGT we estimated may favor this crystal compared to well-known nonlinear crystals. Finally we directly measured the third-order nonlinear electric susceptibility of LGT and determined the corresponding value of the nonlinear refractive index n_2 of LGT. Further investigations will study the experimental parametric gain and evaluate the potential of LGT for large aperture high beam quality OPA in the femtosecond regime.

Funding. This project received funding from the ANR (ANR-10-IDEX-03-02), the ANR-ASTRID (ANR-15-ASTR-0005), ELI-ALPS GOP-1.1.1-12/B-2012-0001, Laserlab-Europe EU-H2020 654148, FEMTO and CMDO+ CNRS Networks.

Acknowledgments. The authors thank Raphaël Clady and Olivier Uteza for their work on the experimental setup, and Jérôme Debray for the orientation and cutting of LGT slabs.

References

1. J. Darginavičius, N. Garejev, and A. Dubietis, *Opt. Lett.* **37**, 4805 (2012).
2. Y. Shamir, J. Rothhardt, S. Hädrich, S. Demmler, M. Tschernajew, J. Limpert, and A. Tünnermann, *Opt. Lett.* **40**, 5546 (2015).
3. J. Nillon, S. Montant, G. Machinet, and E. Cormier, *Lasers, Sources, Relat. Photonic Devices AW5A.3* (2012).
4. F. M. Lu, T. Kanai, Y. Matsumoto, N. Ishii, and J. Itatani, *CLEO, JTu5A.72* (2016).
5. G. Andriukaitis, T. Balčiūnas, S. Ališauskas, A. Pugžlys, A. Baltuška, T. Popmintchev, M.-C. Chen, M. M. Murnane, and H. C. Kapteyn, *Opt. Lett.* **36**, 2755 (2011).
6. G. M. Archipovaite, S. Petit, J.-C. Delagnes, and E. Cormier, *Opt. Lett.* **42**, 891 (2017).
7. D. Brida, C. Manzoni, G. Cirmi, M. Marangoni, S. De Silvestri, and G. Cerullo, *Opt. Express* **15**, 15035 (2007).
8. C. Erny, L. Gallmann, and U. Keller, *Appl. Phys. B* **96**, 257 (2009).
9. M. Baudisch, H. Pires, H. Ishizuki, T. Taira, M. Hemmer, and J. Biegert, *J. Opt.* **17**, 94002 (2015).
10. B. W. Mayer, C. R. Phillips, L. Gallmann, and U. Keller, *Opt. Express* **22**, 20798 (2014).
11. M. Seidel, X. Xiao, A. Hartung, O. Pronin, and F. Krausz, *ASSL, AM3A.7* (2015).
12. J. Stade, L. Bohaty, M. Hengst, and R. B. Heimann, *Crystal Research and Technology* **37**, 1113 (2002).
13. E. Boursier, P. Segonds, B. Boulanger, C. Félix, J. Debray, D. Jegouso, B. Ménaert, D. Roshchupkin, and I. Shoji, *Optics Letters* **39**, 4033 (2014).
14. C. Pasquier, P. Blandin, R. Clady, N. Sanner, M. Sentis, O. Utéza, Y. Li, and S. Yan long, *Optics Communications* **355**, 230 (2015).
15. B. C. Stuart, M. D. Feit, S. Herman, A. M. Rubenchik, B. W. Shore, and M. D. Perry, *J. Opt. Soc. Am. B* **13**, 459 (1996).
16. A. Royon, B. Bousquet, L. Canioni, M. Treguer, T. Cardinal, E. Fargin, D.-G. Kim, and S.-H. Park, *Journal of Optical Society of Korea* **10**, 188 (2006).
17. C. Bosshard, U. Gubler, P. Kaatz, W. Mazerant, and U. Meier, *Phys. Rev. B* **61**, 10688 (2000).
18. H. P. Li, C. H. Kam, Y. L. Lam, W. Ji, *Optical Materials* **15**, 237 (2001).

Full references:

1. J. Darginavičius, N. Garejev, and A. Dubietis, "Generation of carrier-envelope phase-stable two optical-cycle pulses at 2 μm from a noncollinear beta-barium borate optical parametric amplifier.," *Opt. Lett.* **37**, 4805–7 (2012).
2. Y. Shamir, J. Rothhardt, S. Hädrich, S. Demmler, M. Tschernajew, J. Limpert, and A. Tünnermann, "High-average-power 2 μm few-cycle optical parametric chirped pulse amplifier at 100 kHz repetition rate," *Opt. Lett.* **40**, 5546–5549 (2015).
3. J. Nillon, S. Montant, G. Machinet, and E. Cormier, "Phase-stabilized Few-cycle Optical Parametric Amplification at 2.1 μm with 10 μJ at 100 kHz," *Lasers, Sources, Relat. Photonic Devices AW5A.3* (2012).
4. F. M. Lu, T. Kanai, Y. Matsumoto, N. Ishii, and J. Itatani, "KTA-Based Optical Parametric Amplifiers for MJ-Class Mid-IR Source," *CLEO, JTu5A.72* (2016).
5. G. Andriukaitis, T. Balčiūnas, S. Ališauskas, A. Pugžlys, A. Baltuška, T. Popmintchev, M.-C. Chen, M. M. Murnane, and H. C. Kapteyn, "90 GW peak power few-cycle mid-infrared pulses from an optical parametric amplifier.," *Opt. Lett.* **36**, 2755–7 (2011).
6. G. M. Archipovaite, S. Petit, J.-C. Delagnes, and E. Cormier, « 100 kHz Yb-fiber laser pumped 3 μm optical parametric amplifier for probing solid-state systems in the strong field regime, » *Opt. Lett.* **42**(5), 891-894 (2017).
7. D. Brida, C. Manzoni, G. Cirri, M. Marangoni, S. De Silvestri, and G. Cerullo, "Generation of broadband mid-infrared pulses from an optical parametric amplifier.," *Opt. Express* **15**, 15035–40 (2007).
8. C. Erny, L. Gallmann, and U. Keller, "High-repetition-rate femtosecond optical parametric chirped-pulse amplifier in the mid-infrared," *Appl. Phys. B* **96**, 257–269 (2009).
9. M. Baudisch, H. Pires, H. Ishizuki, T. Taira, M. Hemmer, and J. Biegert, "Sub-4-optical-cycle, 340 MW peak power, high stability mid-IR source at 160 kHz," *J. Opt.* **17**, 94002 (2015).
10. B. W. Mayer, C. R. Phillips, L. Gallmann, and U. Keller, "Mid-infrared pulse generation via achromatic quasi-phase-matched OPCPA," *Opt. Express* **22**, 20798–808 (2014).
11. M. Seidel, X. Xiao, A. Hartung, O. Pronin, and F. Krausz, "Multi-Watt MHz-rate Femtosecond Mid-Infrared Source," *ASSL, AM3A.7* (2015).
12. J. Stadel, L. Bohaty, M. Hengst, and R. B. Heimann, "Electro-optic, Piezoelectric and Dielectric Properties of Langasite (La₃Ga₅SiO₁₄), Langanite (La₃Ga₅Nb_{0.5}O₁₄) and Langataite (La₃Ga₅Ta_{0.5}O₁₄)," *Crystal Research and Technology* **37** (10), 1113 (2002).
13. E. Boursier, P. Segonds, B. Boulanger, C. Félix, J. Debray, D. Jegouso, B. Ménaert, D. Roshchupkin, and I. Shoji, "Phase-matching directions, refined Sellmeier equations, and second-order nonlinear coefficient of the infrared Langatate crystal La₃Ga₅Ta_{0.5}O₁₄," *Optics Letters* **39** (13), 4033 (2014).
14. C. Pasquier, P. Blandin, R. Clady, N. Sanner, M. Sentis, O. Utéza, Y. Li, and S. Yan long, "Handling beam propagation in air for nearly 10-fs laser damage experiments," *Optics Communications* **355**, 230 (2015).
15. B. C. Stuart, M. D. Feit, S. Herman, A. M. Rubenchik, B. W. Shore, and M. D. Perry, "Optical ablation by high-power short-pulse lasers," *J. Opt. Soc. Am. B* **13** (2), 459 (1996).
16. A. Royon, B. Bousquet, L. Canioni, M. Treguer, T. Cardinal, E. Fargin, D-G. Kim, and S-H Park, "Third-harmonic generation microscopy for material characterization," *Journal of Optical Society of Korea* **10** (4), 188 (2006).
17. M. Sheik-Bahae, D. Crichton Hutchings, D. J. Hagan, and E. W. Van Stryland, *IEEE J. Quantum Electron.* **27**, 1296 (1991).
18. H. P. Li, C. H. Kam, Y. L. Lam, W. Ji, « Femtosecond Z-scan measurements of nonlinear refraction in nonlinear optical crystals », *Optical Materials* **15**, 237 (2001).